EUROPEAN JOURNAL OF CANCER 47 (2011) 1276–1284

available at www.sciencedirect.com

ScienceDirect

journal homepage: www.ejconline.com

Microvascular biodistribution of L19-SIP in angiogenesis targeting strategies

Marcus Czabanka [a], *Güliz Parmaksiz* [a], *Simon H. Bayerl* [a], *Melina Nieminen* [a], *Eveline Trachsel* [b], *Hans D. Menssen* [d], *Ralf Erber* [c], *Dario Neri* [b], *Peter Vajkoczy* [a,*]

[a] *Department of Neurosurgery, Universitätsmedizin Charitè, Campus Virchow Klinikum, Augustenburger Platz 1, 13353 Berlin, Germany*
[b] *Institute of Pharmaceutical Sciences, Department of Chemistry and Applied Biosciences, Swiss Federal Institute of Technology Zürich, HCI G 392.4, Wolfgang-Pauli-Str., 10 8093 Zürich, Switzerland*
[c] *Department of Orthodontics and Dentofacial Orthopaedics, Dental School, University of Heidelberg, Im Neuenheimer Feld 400, 69120 Heidelberg, Germany*
[d] *Philogen S.P.A, Localita Bellaria 35, 53018 Sovicille, Italy*

ARTICLE INFO

Article history:
Received 14 September 2010
Received in revised form 31 January 2011
Accepted 3 February 2011
Available online 9 March 2011

Keywords:
Antibody-based vascular targeting
L19-SIP
Extra domain B of fibronectin
Angiogenesis
Anti-angiogenic therapy

ABSTRACT

Introduction: Various strategies using L19-mediated fibronectin targeting have become useful clinical tools in anti-tumour therapy and diagnostics. The aim of our study was to characterise the microvascular biodistribution and binding process during tumour angiogenesis and after anti-angiogenic therapy.

Materials and methods: SF126 glioma and F9 teratocarcinoma cells were implanted into dorsal skin fold chambers (SF126: $n = 4$; F9: $n = 6$). Using fluorescence and confocal intravital microscopy the biodistribution process was assessed at $t = 0$ h, $t = 4$ h and $t = 24$ h after intravenous application of Cy3-L19-SIP. Sunitinib treatment was applied for six days and microscopy was performed 2 and 6 days after treatment initiation. Analysed parameters included: vascular and interstitial binding, preferential binding sites of L19-SIP, microvascular blood flow rate, microvascular permeability. Histological analysis included CD31 and DAPI.

Results: L19-SIP showed a specific and time-dependent neovascular binding with a secondary extravasation process reaching optimal vascular/interstitial binding ratio 4 hours after iv administration (F9: L19-SIP: vascular binding: 74.6 ± 14.5; interstitial binding: 46.8 ± 12.1; control vascular: 22,2 ± 16.6). Angiogenic sprouts were preferred binding sites (F9: L19-SIP: 188 ± 15.5; RTV: 90.6 ± 13.5). Anti-angiogenic therapy increased microvascular hemodynamics (SF126: Su: 106.6 ± 13.3 μl/sec; Untreated: 19.7 ± 9.1 μl/sec) and induced increased L19-SIP accumulation (SF 126: t24; Su: 92.6 ± 2.7; Untreated: 71.9 ± 5.9) in therapy resistant tumour vessels.

Conclusion: L19-SIP shows a time and blood-flow dependent microvascular biodistribution process with angiogenic sprouts as preferential binding sites followed by secondary extravasation of the antibody. Microvascular biodistribution is enhanced in anti-angiogenic-therapy resistant tumour vessels.

* *Corresponding author:* Tel.: +4930450560001; fax: +4930450560900
E-mail address: peter.vajkoczy@charite.de (P. Vajkoczy).
0959-8049/$ - see front matter
doi:10.1016/j.ejca.2011.02.001

1. Introduction

Antibody-based targeted delivery of pharmaceuticals has become a promising approach for specifically targeting and supplying diagnostic and therapeutic molecules to solid tumours.[1] The Extradomain B (ED-B) of fibronectin represents one of the most promising neovascular markers. It is typically absent in human plasma and normal adult tissues, but it is strongly expressed in the vasculature of aggressive tumours.[1,2] The antibody L19-SIP has been generated to specifically target the ED-B of fibronectin.[3] Immunocytokines coupled to L19 have been demonstrated to significantly inhibit tumour growth and metastasis.[4] Research has led to the clinical introduction of L19-based targeting strategies. Clinical reports show that the use of L19 is safe and feasible in head and neck squamous cell carcinoma in human patients[5] and that 131I-L19SIP radioimmunotherapy may be successfully applied in Hodgkin lymphoma patients.[6]

Despite growing experimental and clinical experience with L19, its microvascular biodistribution characteristics are not fully understood. However, microvascular biodistribution is of major importance for an adequate understanding of clinical applications of L19 based targeting strategies as there are several physiologic barriers to the delivery of macromolecules in tumours.[7] It was the aim of our study to visualise and characterise the microvascular binding and biodistribution properties of the L19-SIP in two distinct tumour models i.e. F9 teratocarcinoma and a SF126 glioma model.

2. Material and methods

2.1. Tumour cell lines

Murine F9 teratocarcinoma cells and human SF126 glioma cells were grown in DMEM with 4.5 g/L Glucose supplemented with 10% faetal bovine serum (PAA GmbH, Linz, Austria) at 37 °C in 5% CO_2 humidified incubators following conventional protocols.

2.2. Dorsal skinfold chamber model

For the assessment of tumour microvascularisation, F9 teratocarcinoma cells were implanted into dorsal skinfold chambers in C57/B6 mice ($n = 6$ per group) and SF126 glioma cells were implanted in nude mice ($n = 4$ per group) followed by intravital microscopy.

Intravital microscopic analysis was performed on day 14 after F9-teratocarcinoma implantation (during the application of L19-SIP) and on day 7 after SF126 glioma cell implantation. Different starting points were chosen to guarantee sufficient vascularisation in both tumour models because F9 teratocarcinoma demonstrates slower growth dynamics as SF126 gliomas. Microscopy was performed during injection of L19-SIP ($t = 0$) as well as 4 h ($t = 4$h) and 24 h ($t = 24$h) after intravenous application.

The microsurgical techniques for the implantation of the dorsal skinfold chamber have been previously described in detail.[8] All the experiments were approved by the Regierungspräsidium Karlsruhe and were carried out according to the guidelines for animal care and experimentation.

2.3. Intravital-microscopy

Mice were anesthetised by intraperitoneal injection with a mixture of ketamine (100 mg/kg) and xylazine (10 mg/kg). Intravital fluorescence video microscopy (IFVM) was performed by epi-illumination techniques using a modified Axiotech vario microscope (Attoarc; Zeiss, Jena, Germany). Microscopic images were recorded through a charge-coupled device (CCD) video camera with an optional image intensifier for weak fluorescence (Kappa, Gleichen, Germany) and transferred to a S-VHS video system (Panasonic) for offline analysis. Offline analysis was performed using a computer assisted analysis system (CAPIMAGE; Zeintl Software Engineering, Heidelberg, Germany). Microvessels were visualised by contrast enhancement with 2% FITC-conjugated dextran (0.1 ml, intravenous; molecular weight 150,000; Sigma). Simultaneous *in vivo* application of the Cy3-labelled L19-SIP and the use of green-light epi-illumination allowed for sequential analysis of biodistribution. Microvascular permeability (P) calculated as the ratio between intra- and extravascular contrast as described previously.[8,9]

2.4. Biodistribution analysis

In order to study microvascular biodistribution of L19-SIP, we injected 100 μg of Cy3-labelled L19-SIP (SIP group) into the jugular vein of animals. Animals without implanted tumour cells in the chamber served as SIP-control group. Cy3-L19-SIP was injected intravenously in order to visualise L19-SIP biodistribution in host vasculature.

Biodistribution was studied by measuring fluorescence intensity in the vascular and interstitial compartment in a total number of 6–9 tumour vessels per animal. For the measurement of fluorescence intensity we defined 2 regions of interest (area: 250–500 μm^2) per analysed tumour vessel: (i) the vascular compartment referring the vascular wall and the close perivascular area (defined as an area of 250–500 μm^2 with a width of 3 μm located next to the analysed tumour vessel) and (ii) the interstitial compartment (area of 250–500 μm^2) located in the interstitial space with a distance of 20 μm from the analysed tumour vessel. Before injection, we measured interstitial fluorescence intensity in order to exclude autofluorescent activity.

2.5. Biodistribution analysis during antiangogenic therapy

In order to analyse the influence of antiangiogenic therapy on microvascular biodistribution of L19-SIP, SF126 glioma cells were implanted into dorsal skinfold chambers in nude mice ($n = 4$ per group). As antiangiogenic agent we used the multi-kinase inhibitor Sunitinib. This model has been described as very suitable for IFVM.[10] Treatment with Sunitinib was initiated 7 days after SF 126 glioma cell implantation. All the animals in the treatment group received daily intraperitoneal injections of Sunitinib (40 mg/kg/day) for 6 days. Control animals received daily injections of 0.9% NaCl. IFVM was performed on day 2 and 6 after the initiation of treatment. For analysis of tumour microhemodynamics we assessed microvascular red blood cell velocity (RBCV;

mm/s) and microvascular blood flow rate (Q_v; nL/s) as described previously.[8,11]

2.6. Intravital confocal laser scanning microscopy

Intravital confocal laser scanning microscopy (ICLSM) offers specific advantages over epiillumination techniques including the ability to control depth of field and the capability to collect serial optical sections from thick specimens. In order to characterise the localisation of L19-SIP accumulation, we performed ICLSM on F9 teratocarcinoma tumours in dorsal skinfold chambers implanted in C57/B6 mice ($n = 4$). Fluorescence images were acquired with a Leica TCPSP2 confocal scanning laser microscope (CSLM; Leica, Bensheim, Germany). Images were acquired with an in-plane resolution of 512 by 512 pixels.

Tumour vasculature was visualised by injecting 2% FITC-labelled 150 kDa dextran (100 μl, i.v). Z stacks were collected through about 100 μm of tumour tissue with a z-step interval of 5 μm. Average projections of the stacks were generated using the image acquisition and processing software of the manufacturer.

2.7. Immunofluorescence staining

Cryosections (4 μm) of Cy3-L19-SIP- injected SF126 glioma tumours (collected at day 1 after injection) were fixed with Acetone and stained for CD31 using rat monoclonal antibody MEC13.3 (BD Pharmingen, Heidelberg, Germany) in combination with a FITC conjugated donkey-anti-rat secondary antibody (Dianova, Hamburg, Germany). Sections were mounted with immunoselect antifading mounting medium DAPI (Dianova, Hamburg, Germany) including the staining of nuclei. 5 μm cryosections of Cy3-L19-SIP injected F9 teratocarcinoma tumours were fixed with 4%PFA and stained for CD31 using the rat monoclonal antibody MEC13.3 (BD Pharmingen, Heidelberg, Germany) in combination with an anti-rat-Cy2-labelled secondary antibody (Dianova, Hamburg, Germany). Staining of the nuclei was performed using DAPI, sections were mounted with elvanol. Colocalisation of the Cy3-L19-SIP signal and the CD31 signal was observed using an Axioplan2 Imaging microscope (Zeiss, Jena, Germany). Photomicrographs were acquired and processed using the Axiovision software package (Zeiss, Jena, Germany)

2.8. Statistical analysis

Quantitative data are given as mean ± SD. Mean values of all parameters were calculated from the average values in each animal. For analysis of differences between groups Students t-test was performed. Results with $p < 0.05$ were considered significant.

3. Results

3.1. Biodistribution of L19-SIP

Using IFVM a clear vascular binding pattern is demonstrated with L19-SIP binding specifically to neoangiogenic vessels. In host vasculature no significant antibody binding could be detected (Fig. 1). ICLSM confirmed the spatial distribution of vascular specific L19-SIP binding by showing Cy3-L19-SIP fluorescence in tumour vessels (Fig. 1). By 3D-reconstructing the images and comparing different depths of microscopy we were able to exactly localise the fluorescent signal in the vascular wall and close perivascular area (Fig. 1C)

During injection of Cy3-L19-SIP we did not observe antibody binding to the vascular wall. After 4 hours IFVM demonstrated significantly increased antibody binding in the vascular wall and close perivascular area (Fig. 2). This binding process declined subsequently over the remaining experimental period in both tumour models but still remained significantly higher compared to baseline (Fig. 2B and C). Furthermore, L19-SIP was found to extravasate into tumour interstitium. The extravasation process was stronger in SF126 gliomas as compared to F9 teratocarcinomas (Figs. 2B and C). Considering the declining vascular fluorescence signal, the best signal-to-noise ratio between the vascular and interstitial compartment was reached 4 h after injection of L19-SIP (Fig. 3). This effect was more pronounced in F9 teratocarcinomas resulting in a significantly superior signal to noise ratio as compared to SF 126 gliomas (Fig. 3C). As extravasation of L19-SIP may be influenced by microvascular permeability, microvessels of SF126 gliomas were characterised by a significantly increased permeability index as compared to F9 teratocarcinoma microvessels. Because permeability index is defined as intravascular fluorescence intensity/extravascular fluorescence intensity, SF126 glioma vessels demonstrated significantly increased extravasation and therefore increased permeability (Fig. 3D).

Immunohistochemistry confirmed the spatial distribution of CY3-L19-SIP predominantly in the vascular wall and close perivascular area in both tumour entities (Fig. 3E). It demonstrated secondary interstitial accumulation with a reduced fluorescence signal in the interstitial space.

3.2. L19-SIP preferentially binds to angiogenic sprouts

IFVM revealed significantly enhanced microvascular binding of L19-SIP to vascular sprouts (Fig. 4). Vascular sprouts were identified as non-connected, dead end, non-red blood cell perfused vascular structures that form at sites of neovascularisation from existing red-blood cell perfused blood vessels.[12] Quantification of fluorescence intensity confirmed this observation by demonstrating a 2-fold increase in vascular L19-SIP uptake in vascular sprouts as compared to the remaining tumour vasculature (Fig. 4). This observation suggests a high affinity of L19-SIP for immature, plastic blood vessels.

3.3. Antiangiogenic therapy enhances microvascular binding

In order to analyse the biodistribution of L19-SIP during antiangiogenic therapy, we used the SF126 glioma model with Sunitinib therapy. With this approach, treated tumours demonstrated a microvessel density of 128.5 ± 19.4 cm/cm^2 compared to placebo treated tumours which showed a microvessel density of 338.1 ± 37.4 cm/cm^2 after the treatment period of 6 days (data not shown). During the early phase (initial 48 hours) of Sunitinib treatment no significant alteration in

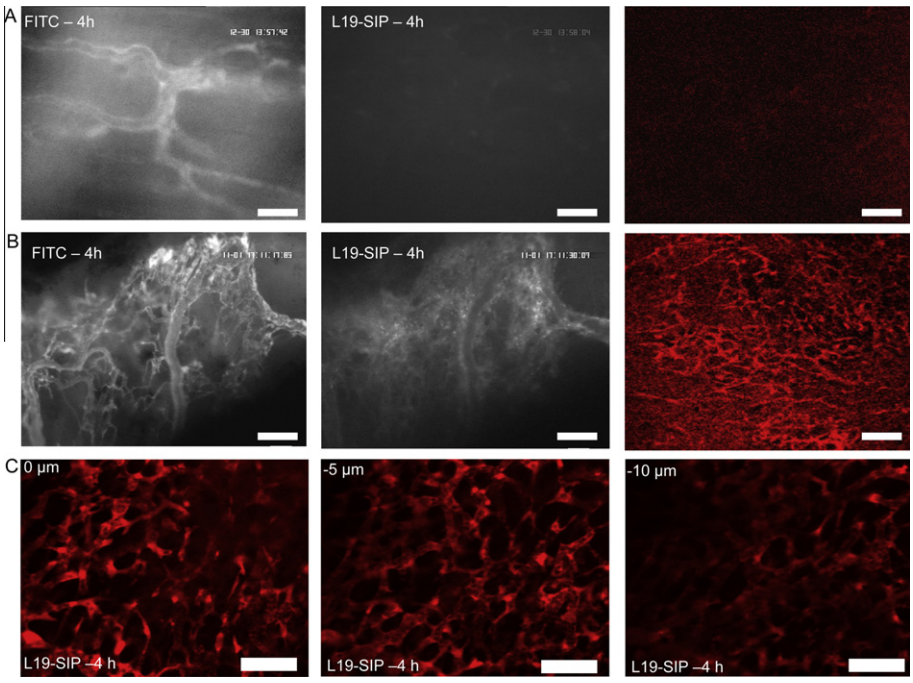

Fig. 1 – (A) Left image: Characteristic intravital microscopic image of postcapillary venules of host vasculature 4 hours after intravenous administration of CY3-L19-SIP during FITC Dextran visualisation; bar indicates 100 μm. Middle image: Intravital microscopic image of corresponding host vasculature during CY3 visualisation showing no fluorescent signal in host vasculature due to missing CY3-L19-SIP binding to microvasculature; bar indicates 200 μm. Right image: Characteristic intravital confocal laser scanning microscopic (ICLSM) image of host vasculature during visualisation of CY3; vascular structures can not be identified due to missing microvascular L19-SIP binding; bar indicates 200 μm. (B) Left image: Characteristic intravital microscopic image of tumour vasculature 4 hours after intravenous administration of CY3-L19-SIP during FITC Dextran visualisation in F9 teratocarcinoma; bar indicates 200 μm. Middle image: Representative intravital image of corresponding tumour vessels during CY3 visualisation showing a clear fluorescent contrast in tumour vasculature due to specific binding of CY3-L19-SIP 4 h after CY3-L19-SIP administration; fluorescent contrast highlights the vascular wall and close perivascular area thereby visualising the vascular angioarchitecture; bar indicates 200 μm. Right image: Characteristic ICLSM image of tumour vasculature during CY3 visualisation in F9 teratocarcinoma; tumour vessel specificity of L19-SIP leads to distinct accumulation of L19-SIP around tumour vessels enabling clear visualisation of vascular structures; bar indicates 200 μm. (C) Left to right image: ICLSM images showing tumour neovasculature in different depths during microscopy exactly localising the fluorescent signal in the vascular wall and close perivascular area in F9 teratocarcinoma; the fluorescent signal clearly depicts vascular structures in the vascular plane (left image: depth 0 μm), whereas the signal slowly fades as the focus leaves the vascular plane towards the interstitial space (middle image: depth −5 μm; right image: depth −10 μm), bars indicate 100 μm.

L19-SIP accumulation was observed (data not shown), whereas vascular and interstitial accumulation of L19-SIP were significantly increased in remaining, therapy resistant tumour vessels after the treatment period (Fig. 5A). Due to the strong reduction of microvessel density in response to antiangiogenic therapy, overall uptake of L19-SIP in tumours was not analysed. We focused on the uptake of L19-SIP in surviving, therapy resistant tumour vessels in order to characterise L19-SIP hot spots after antiangiogenic therapy. Increased L19 SIP uptake in resistant tumour vessels and increased extravasation became apparent 4 h after injection of the antibody and remained during the entire experiment. Immunohistochemistry showed that localisation of ED-B epitope was not altered by therapy (Fig. 5A–D). Increased vascular accumulation may depend on microvascular delivery of the antibody and associated microhemodynamics. Microhemodynamic analysis revealed that increased vascular and interstitial accumulation of L19-SIP was parallelled by significantly enhanced microvascular blood flow rate in therapy-resistant tumour vasculature (Fig. 5E).

4. Discussion

We show novel biodistribution characteristics for L19-SIP by demonstrating that L19-SIP specifically targets tumour vessels in a time and blood flow dependent manner with specific binding sites and secondary extravasation into tumour interstitium. Antiangiogenic treatment enhances microvascular accumulation of L19-SIP in therapy resistant tumour vessels potentially by improving microhemodynamics and consequently enhancing microvascular delivery of L19-SIP.

Targeting tumour vessels using specific angiogenic markers has become a promising approach to refine and promote anti-tumour strategies.[4,13,14] Currently several clinical trials

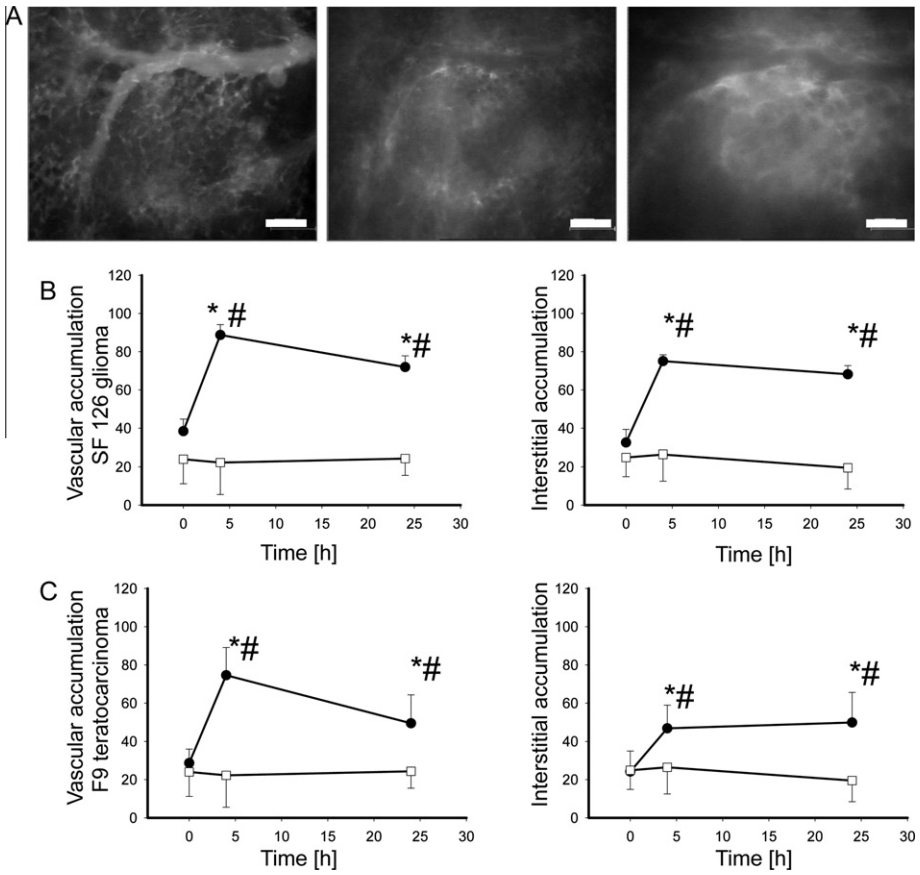

Fig. 2 – (A) Left image: Representative intravital microscopic image of tumour vessels after FITC administration visualising tumour microvasculature in F9 teratocarcinoma; bar indicates 200 μm. Middle image: Representative intravital microscopic image of the corresponding tumour vessel using CY3 visualisation 4 h after iv administration of CY3-L19-SIP; the vascular wall and the close perivascular area show distinct fluorescence signal in contrast to the slight fluorescence signal in the surrounding interstitium; an optimal signal-to-noise ratio enables clear visualisation of tumour vessels; bar indicates 200 μm. Right image: Intravital confocal laser scanning microscopic (ICLSM) image of the corresponding tumour vessel using CY3 visualisation 24 h after iv administration of CY3-L19-SIP; due to extravasation of L19-SIP into tumour interstitium and decreasing vascular binding the signal-to-noise ratio is decreased; therefore tumour vessels can not be clearly depicted during intravital microscopy; bar indicates 200 μm. (B) Quantification of fluorescence intensity in the vascular compartment (left graph) and in the interstitial compartment (right graph) in SF126 glioma; * = $p < 0.05$ versus control; # = $p < 0.05$ versus baseline; $n = 4$; black circles = tumour group, white squares = control group, unit = fluorescence grey values. (C) Quantification of fluorescence intensity in the vascular compartment (left graph) and in the interstitial compartment (right graph) in F9 teratocarcinoma; * = $p < 0.05$ versus control; # = $p < 0.05$ versus baseline; $n = 6$; black circles = tumour group, white squares = control group, unit = fluorescence grey values.

are conducted using L19-coupled therapy strategies.[4] In the face of ongoing clinical trials, our study investigates the microvascular biodistribution process of the antibody fragment L19-SIP. IFVM allows real-time, online, *in vivo* assessment of antibody accumulation on a microvascular level and consequently represents an ideal tool for biodistribution analysis. Our study verifies the selectivity of L19-SIP for neoangiogenic tumour vessels. These results are supported by previous reports demonstrating selective vascular targeting using L19-SIP in other experimental tumour models.[1,15,16] The binding process follows specific kinetics, with a decline in vascular binding after an initial steep incline reaching its maximum 4 hours after intravenous injection of L19-SIP. Results from Borsi et al. support our results by demonstrating maximum intratumoural accumulation of L19-SIP occuring 4–6 hours after intravenous application in a F9 teratocarcinoma model.[3] Additionally, we show that L19-SIP extravasates into tumour interstitium in a secondary process. This extravasation process leads to an optimal signal-to noise ratio occurring in both of our tumour models 4 hours after application of the antibody. Tumour-specific pathophysiological features may explain this observation. In our model, F9 teratocarcinomas were characterised by lower permeability and a better signal-to-noise ratio for L19-SIP. Signal-to-noise ratio is defined as the ratio of the vascular and the interstitial accumulation of L19-SIP. According to this definition, the signal-to-noise ratio is decreased if extravasation and therefore interstitial accumulation of L19-SIP is increased. Consequently, F9 teratocarcinoma might show a better signal to noise ratio due to less extravasation as a result of reduced

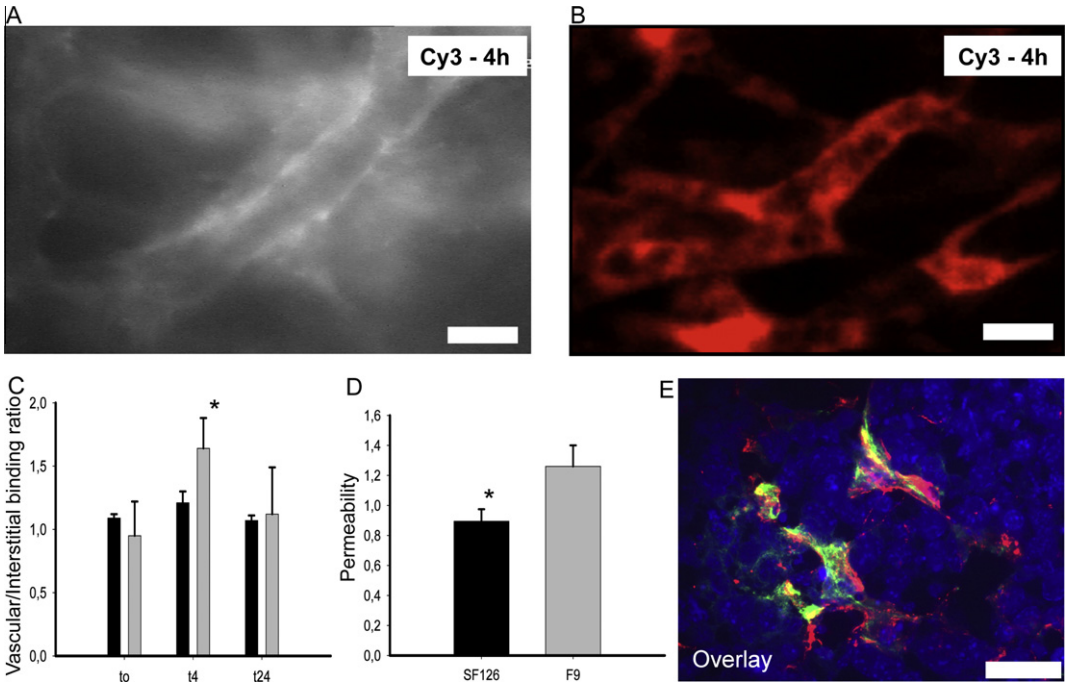

Fig. 3 – (A) Representative intravital microscopic image of tumour vasculature during CY3 visualisation demonstrating the optimal signal-to-noise ratio between the vascular and interstitial compartment 4 hours after intravenous application of the L19-SIP (due to distinct fluorescence of perivascular area in contrast to slight fluorescence intensity in interstitium) in F9 teratocarcinoma; bar indicates 50 μm. (B) Representative intravital confocal laser scanning microscopic image of tumour vasculature during CY3 visualisation demonstrating the optimal signal-to-noise ratio between the vascular and interstitial compartment 4 hours after intravenous application of the antibody fragment in F9 teratocarcinoma; bar indicates 50 μm. (C) F9 teratocarcinomas shows a significantly higher vascular/interstitial binding ratio compared to SF126 gliomas 4 hours after intravenous application of L19-SIP; * = $p < 0.05$ versus SF126 glioma; F9 teratocarcinoma: $n = 6$, SF126 glioma: $n = 4$; grey columns indicate F9 teratacarcinoma, black columns indicate SF126 glioma. (D) Quantification of permeability index of both tumour models. A decreased permeability index highlights an increased microvascular permeability (permeability index = intravascular/extravascular fluorescence). SF 126 glioma show a significantly decreased permeability index (i.e. higher microvascular permeability) as compared to F9 teratocarcinoma; * = $p < 0.05$ versus SF126 glioma; F9 teratocarcinoma: $n = 6$, SF126 glioma: $n = 4$; grey columns indicate F9 teratacarcinoma, black columns indicate SF126 glioma. (E) Immunohistochemistry staining demonstrating spatial distribution of CY3-L19-SIP (red fluorescence signal) around vascular structures (yellow fluorescence signal) amongst F9 tumour cells (blue fluorescence signal); bar indicates 20 μm. (For interpretation of the references to colour in this figure legend, the reader is referred to the web version of this article.)

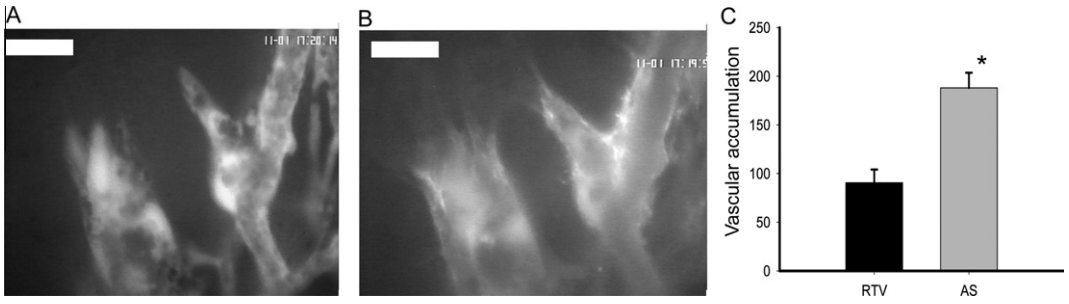

Fig. 4 – (A+B) Representative intravital microscopic images of vascular sprouts during FITC-visualisation (A) and during CY3 visualisation (B) showing dense fluorescence signal in the vascular wall and perivascular area around vascular sprouts 4 h after iv administration of CY3-L19-SIP in F9 teratocarcinoma; bars indicate 50 μm. (C) Quantification of CY3-L19-SIP binding in microvascular sprouts demonstrating a significant difference between fluorescence intensity in angiogenic sprouts (AS) compared to fluorescence intensity in remaining tumour vessels (RTV) in F9 teratocarcinoma; * = $p < 0.05$ versus RTV; $n = 6$.

permeability. However, extravasation of molecules depends on a variety of mechanisms and differences in permeability may not be the only underlying mechanism. Fibronectin expression in interstitium, differences in interstitial diffusion coefficient and high hydraulic conductivity may influence this extravasation process.[7]

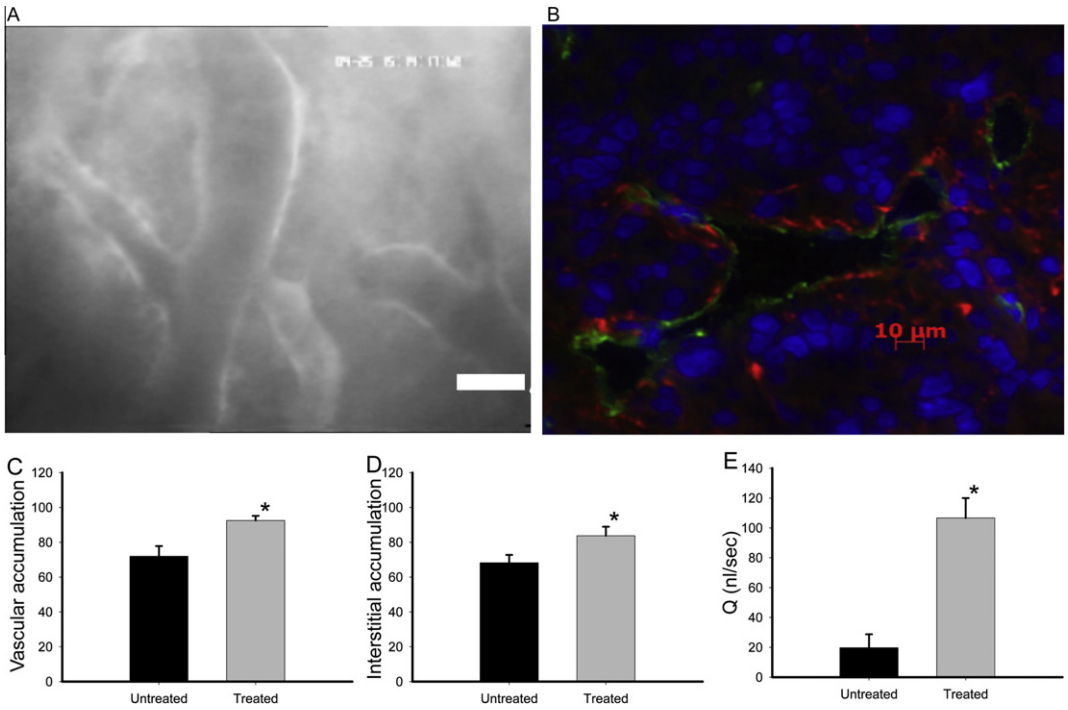

Fig. 5 – (A) Characteristic intravital microscopic image of therapy resistant tumour vessels during Cy3 visualisation 4 hours after Cy3-L19-SIP administration indicating significantly enhanced vascular and interstitial accumulation of L19-SIP after Sunitinib treatment in SF126 glioma, bar indicates 100 μm. (B) Representative immunohistochemical image of Sunitinib treated tumours demonstrating the localisation of the Cy3-L19-SIP (red fluorescence) in extracellular matrix surrounding endothelial cell marker FITC-CD31 (green fluorescence) amongst SF126 tumour cells (blue fluorescence) 1 day after Cy3-L19-SIP administration in SF126 glioma. (C+D) Quantification of CY3-L19-SIP vascular (C) and interstitial (D) binding in Sunitinib treated SF126 gliomas showing a significant enhancement compared to untreated tumours 24 h after Cy3-L19-SIP administration.; * = $p < 0.05$ versus untreated; $n = 4$. (E) Quantification of blood flow rate in untreated and therapy resistant tumour vessels showing a significant improvement of microvascular blood flow in therapy resistant tumour vessels compared to untreated tumour vessels in SF126 glioma; * = $p < 0.05$ versus untreated; $n = 4$. (For interpretation of the references to colour in this figure legend, the reader is referred to the web version of this article.)

In response to antiangiogenic treatment, we demonstrate increased microvascular accumulation of L19-SIP. In this context we show that antiangiogenic treatment does not change the localisation of the ED-B epitope. In both untreated and treated tumour vessels, ED-B of fibronectin was predominantly located on the abluminal side of the vascular wall. Nevertheless, the microvascular distribution of antibodies in tumours depends on a variety of microvascular and microenvironmental factors.[7] One of the most important factors is microvascular blood flow. It has been established that tumours are characterised by very heterogenous zones of high- and low blood flow areas.[17] We have shown previously that Sunitinib treatment leads to a strong increase in microvascular blood flow rate in therapy-resistant tumour vessels and a homogenisation of tumour microcirculation leading to improved delivery of chemotherapy.[10] Improved delivery of L19-SIP to the epitope might explain the increased vascular accumulation of L19-SIP in treated tumour vessels. Similar effects may be observed using other antiangiogenic compounds with a similar target profile such as Sorafenib. However, our study can not address whether molecular upregulation and increased expression of the epitope in the individual, Sunitinib-resistant vessels contribute to our observation. This might represent another potential mechanism, even though the presented results herein suggest that L19-SIP preferentially targets immature, plastic blood vessels. The concept of vascular normalisation,[18] which postulates that blood vessels become more mature in response to anti-angiogenic treatment, would contradict this hypothesis.

We identified angiogenic sprouts as preferential binding sites for L19-SIP. Sprouting angiogenesis depends on selection of a tip cell destined to lead the sprout into the tissue and anastomose with other vessels to complete a vascular loop.[19] In this scenario fibronectin represents a major component of the provisional extracellular matrix of growing microvessels as migrating and proliferating endothelial cells have been shown to produce the appropriate matrix including fibronectin.[20] Vascular sprouts may represent preferential binding sites for L19-SIP due to the strong remodelling process of the extracellular matrix during microvascular sprout formation.

Even though the results of animal models may not be completely translated into the human pathophysiologic setting especially regarding intratumoural and peritumoural vasculature,[21] glioma tumour cells have been attributed a deciding role in determining tumour vessel characteristics.[22,23] Therefore, our study provides data that might be translated into

clinical applications. From a translational point of view, our data imply that tumours with a high angiogenic activity and a strong vascular turnover may represent preferred L19-SIP targets due to the high angiogenic potential. In this scenario, L19-SIP will bind to well-perfused tumour areas, whereas weakly-perfused areas will not be targeted to the same extent. This hemodynamic dependency might not only explain therapy resistance to L19-mediated therapy strategies but it opens a mechanism for overcoming therapy resistance and for improving therapy efficacy: antiangiogenic therapy might be used as a tool to change tumour hemodynamics with the potential to improve the efficacy of L19 mediated therapies by increasing the microvascular binding process in therapy resistant tumour vessels. Moreover, we demonstrate extravasation of L19-SIP thereby opening another field of activity for L19 mediated therapy strategies: tumour vessels and, in a reduced setting, tumour interstitium. As antiangiogenic compounds are used with an increasing frequency in oncology, there is currently no sufficient tool to directly monitor the effects of antiangiogenic compounds on tumour microvasculature. Using L19-SIP in a diagnostic setting might allow monitoring of the antianigogenic efficacy of clinically used compounds.

In conclusion we demonstrate that L19-SIP represents a useful tool to specifically target tumour microvessels with preferential binding in angiogenic sprouts and secondary extravasation into tumour interstitium depending in part on tumour specific characteristics like microvascular permeability. Antiangiogenic therapy leads to increased microvascular accumulation of L19-SIP in therapy resistant tumour vessels by increasing microvascular hemodynamics underlining the dependence of the delivery process on microvascular hemodynamics. Therefore, we provide useful insights into the microvascular biodistribution process of L19-SIP that may be used for future clinical applications.

Conflict of interest statement

H.D.M. was a senior director at Bayer Schering Pharma and owns few regular stocks from an employee stock purchase plan since February 2008. Dario Neri is a co-founder and shareholder of Philogen, the biotech company which has in-licensed the L19 antibody from ETH Zurich. The remaining authors declare no competing conflicts of interest.

Funding

This study was funded by the Immuno-PDT consortium and the Berliner Krebsgesellschaft e.V.

Equipment

L19-SIP was provided by D. Neri and E. Trachsel Institute of Pharmaceutical Sciences, Department of Chemistry and Applied Biosciences, Swiss Federal Institute of Technology Zürich, HCI G 392.4. Wolfgang-Pauli-Str. 10 8093 Zürich, Switzerland.

REFERENCES

1. Tarli L, Balza E, Viti F, et al. A high-affinity human antibody that targets tumoral blood vessels. *Blood* 1999;**94**:192–8.
2. Kosmehl H, Berndt A, Strassburger S, et al. Distribution of laminin and fibronectin isoforms in oral mucosa and oral squamous cell carcinoma. *Br J Cancer* 1999;**81**:1071–9.
3. Borsi L, Balza E, Bestagno M, et al. Selective targeting of tumoral vasculature: comparison of different formats of an antibody (L19) to the ED-B domain of fibronectin. *Int J Cancer* 2002;**102**:75–85.
4. Kaspar M, Trachsel E, Neri D. The antibody-mediated targeted delivery of interleukin-15 and GM-CSF to the tumor neovasculature inhibits tumor growth and metastasis. *Cancer Res* 2007;**67**:4940–8.
5. Birchler MT, Milisavlijevic D, Pfaltz M, et al. Expression of the extra domain B of fibronectin, a marker of angiogenesis, in head and neck tumors. *Laryngoscope* 2003;**113**:1231–7.
6. Sauer S, Erba PA, Petrini M, et al. Expression of the oncofetal ED-B-containing fibronectin isoform in hematologic tumors enables ED-B-targeted 131I–L19SIP radioimmunotherapy in Hodgkin lymphoma patients. *Blood* 2009;**113**:2265–74.
7. Jain RK. Physiological barriers to delivery of monoclonal antibodies and other macromolecules in tumors. *Cancer Res* 1990;**50**:814s–9s.
8. Vajkoczy P, Schilling L, Ullrich A, Schmiedek P, Menger MD. Characterization of angiogenesis and microcirculation of high-grade glioma: an intravital multifluorescence microscopic approach in the athymic nude mouse. *J Cereb Blood Flow Metab* 1998;**18**:510–20.
9. Vajkoczy P, Menger MD, Vollmar B, et al. Inhibition of tumor growth, angiogenesis, and microcirculation by the novel Flk-1 inhibitor SU5416 as assessed by intravital multi-fluorescence videomicroscopy. *Neoplasia* 1999;**1**:31–41.
10. Czabanka M, Vinci M, Heppner F, Ullrich A, Vajkoczy P. Effects of sunitinib on tumor hemodynamics and delivery of chemotherapy. *Int J Cancer* 2009;**124**:1293–300.
11. baker M, Wayland H. On-line volume flow rate and velocity profile measurement for blood in microvessels. *Microvasc Res* 1974;**7**:131–43.
12. Vajkoczy P, Farhadi M, Gaumann A, et al. Microtumor growth initiates angiogenic sprouting with simultaneous expression of VEGF, VEGF receptor-2, and angiopoietin-2. *J Clin Invest* 2002;**109**:777–85.
13. Berndorff D, Borkowski S, Moosmayer D, et al. Imaging of tumor angiogenesis using 99mTc-labeled human recombinant anti-ED-B fibronectin antibody fragments. *J Nucl Med* 2006;**47**:1707–16.
14. Balza E, Mortara L, Sassi F, et al. Targeted delivery of tumor necrosis factor-alpha to tumor vessels induces a therapeutic T cell-mediated immune response that protects the host against syngeneic tumors of different histologic origin. *Clin Cancer Res* 2006;**12**:2575–82.
15. Neri D, Carnemolla B, Nissim A, et al. Targeting by affinity-matured recombinant antibody fragments of an angiogenesis associated fibronectin isoform. *Nat Biotechnol* 1997;**15**:1271–5.
16. Kaczmarek J, Castellani P, Nicolo G, et al. Distribution of oncofetal fibronectin isoforms in normal, hyperplastic and neoplastic human breast tissues. *Int J Cancer* 1994;**59**:11–6.
17. Vajkoczy P, Menger MD. Vascular microenvironment in gliomas. *Cancer Treat Res* 2004;**117**:249–62.
18. Jain RK. Antiangiogenic therapy for cancer: current and emerging concepts. *Oncology (Williston Park)* 2005;**19**:7–16.
19. Hellstrom M, Phng LK, Hofmann JJ, et al. Dll4 signalling through Notch1 regulates formation of tip cells during angiogenesis. *Nature* 2007;**445**:776–80.

20. Risau W, Lemmon V. Changes in the vascular extracellular matrix during embryonic vasculogenesis and angiogenesis. *Dev Biol* 1988;**125**:441–50.
21. de Jong M, Maina T. Of mice and humans: are they the same?–Implications in cancer translational research. *J Nucl Med* 2010;**51**:501–4.
22. Coomber BL, Stewart PA, Hayakawa EM, Farrell CL, Del Maestro RF. A quantitative assessment of microvessel ultrastructure in C6 astrocytoma spheroids transplanted to brain and to muscle. *J Neuropathol Exp Neurol* 1988; **47**:29–40.
23. Konerding MA, Fait E, Dimitropoulou C, et al. Impact of fibroblast growth factor-2 on tumor microvascular architecture. A tridimensional morphometric study. *Am J Pathol* 1998;**152**:1607–16.